

# Maximizing the grafting of zwitterions onto the surface of ultrafiltration membranes to improve antifouling properties

Nima Shahkaramipour<sup>a</sup>, Amin Jafari<sup>a</sup>, Thien Tran<sup>a</sup>, Christopher M. Stafford<sup>b</sup>, Chong Cheng<sup>a</sup>, and Haiqing Lin<sup>\*a</sup>

Received 00th January 20xx,  
Accepted 00th January 20xx

DOI: 10.1039/x0xx00000x

Superhydrophilic zwitterions have been extensively exploited for surface modification to improve antifouling properties. However, it remains challenging to form layers of < 20 nm with high zwitterion content on the surfaces with different degrees of hydrophilicity. We demonstrate that amine-functionalized sulfobetaine (SBAm) can be co-deposited with dopamine on ultrafiltration (UF) membranes, leading to a thickness of 10 nm to 50 nm and an SBAm content of up to 31 mass% in the coating layers. The covalently grafted SBAm is stable underwater and improves the antifouling properties, as evidenced by the lower trans-membrane pressure required to retain targeted water fluxes than that required for the pristine membranes. The SBAm is also more effective than conventionally used sulfobetaine methacrylate (SBMA) for the zwitterion grafting on the surface to improve antifouling properties.

## 1. Introduction

Polymeric membranes are widely employed for wastewater treatment due to their superior separation performance and high energy-efficiency. However, membranes are often susceptible to fouling by accumulation of suspended solids and dissolved contaminants, which decreases water permeance.<sup>1-3</sup> An effective strategy to mitigate fouling is to graft hydrophilic materials onto the membrane surface to minimize any favorable interactions between the surface and foulants, such as zwitterions containing cations and anions with neutral charges but superhydrophilicity. For example, zwitterionic materials (ZMs) with acrylate and methacrylate groups were directly copolymerized with membrane materials,<sup>4</sup> deposited on the surface using chemical vapor deposition,<sup>5</sup> or grafted from the surface using surface-initiated polymerization<sup>6-8</sup> or other reactions with the surface.<sup>9-13</sup> However, these processes can involve complex chemistry and are often surface-specific. There is a need for a versatile platform to graft various zwitterions on-demand for different foulants onto membranes with different surface properties.

Bio-inspired dopamine can self-polymerize in aqueous solutions and form insoluble polydopamine (PDA) that can deposit on hydrophilic and hydrophobic polymer surfaces.<sup>14, 15</sup> More importantly, the “adhesive” PDA comprises catechol and amine groups and can be used to incorporate functional ZMs.<sup>16-19</sup> For example, poly(sulfobetaine methacrylate) (polySBMA) can be directly coated on a membrane surface primed by PDA through non-covalent linkages.<sup>20-22</sup> However, the lack of covalent bonds between the PDA and superhydrophilic ZMs presents concerns for long-term underwater operation.

The key to graft ZMs using dopamine is to optimize the

functional groups of the ZMs that can react with PDA to obtain thin layers (without adding significant transport resistance) and high zwitterion content to maximize antifouling properties. Methacrylate-containing ZMs have been co-deposited with dopamine, such as sulfobetaine methacrylate (SBMA), with good stability and hydrophilicity.<sup>18, 19, 23</sup> When 1 g/L dopamine and 4 g/L SBMA was deposited for 8 h (i.e. 4-SBMA/1-Dopa@8h), the SBMA content in the coating layer was only  $\approx$  11 mass%, and increasing the SBMA content from 0 g/L to 4 g/L in the solution had minimal effect on the layer thickness ( $\approx$ 15 nm). By contrast, for  $\gamma$ -SBMA/2-Dopa@8h, increasing the SBMA content ( $\gamma$ ) from 0 g/L to 30 g/L increased the coating layer thickness from  $\approx$ 32 nm to  $\approx$ 59 nm, and the SBMA content in the coating layer was observed to be as high as 34 mass%.<sup>19</sup> However, thick surface layers are not preferred for membrane modification due to the increased resistance for water transport, though it has not been systematically explored to date.

Conversely, amine-containing materials can be co-deposited with dopamine.<sup>14, 24-26</sup> For example, amine-terminated poly(ethylene glycol) (PEG-NH<sub>2</sub>) was grafted onto PDA-functionalized ultrafiltration (UF) membranes and formed a layer of  $\approx$ 300 nm.<sup>27</sup> 4,4'-Azodianiline (AZO) was similarly grafted onto PDA-functionalized membranes to form a layer of 17 to 37 nm.<sup>28</sup> Alternatively, polyethylenimine (PEI) was co-deposited with dopamine to produce nanofiltration (NF) membranes for desalination.<sup>29</sup> However, amine-functionalized ZMs have not been co-deposited with dopamine on the membrane surface and explored for improving antifouling properties.

Herein we demonstrate that sulfobetaine amine (SBAm) can be co-deposited with dopamine onto the surface of a UF membrane, producing thin layers and high zwitterion content that display superior antifouling properties. As shown in Fig. 1, SBAm can react with dopamine monomer/oligomer and thus be incorporated into a stable PDA layer, which is thin and does not significantly block the membrane pores. The products of the SBAm and dopamine in the solutions were analyzed using <sup>1</sup>H NMR and scanning electron microscopy (SEM). The effects of coating conditions (including the composition of coating solutions and coating time) on the thickness and the SBAm

<sup>a</sup> Department of Chemical and Biological Engineering, University at Buffalo, The State University of New York, Buffalo, NY 14260, USA.

<sup>b</sup> Materials Science & Engineering Division, National Institute of Standards and Technology (NIST), 100 Bureau Drive, Gaithersburg, MD 20899, USA.

<sup>c</sup> \* Email: [haiqingl@buffalo.edu](mailto:haiqingl@buffalo.edu); Tel: +1-716-645-1856.

<sup>d</sup> Electronic Supplementary Information (ESI) available: additional NMR, SEM, XPS, and membrane permeance data. See DOI: 10.1039/x0xx00000x

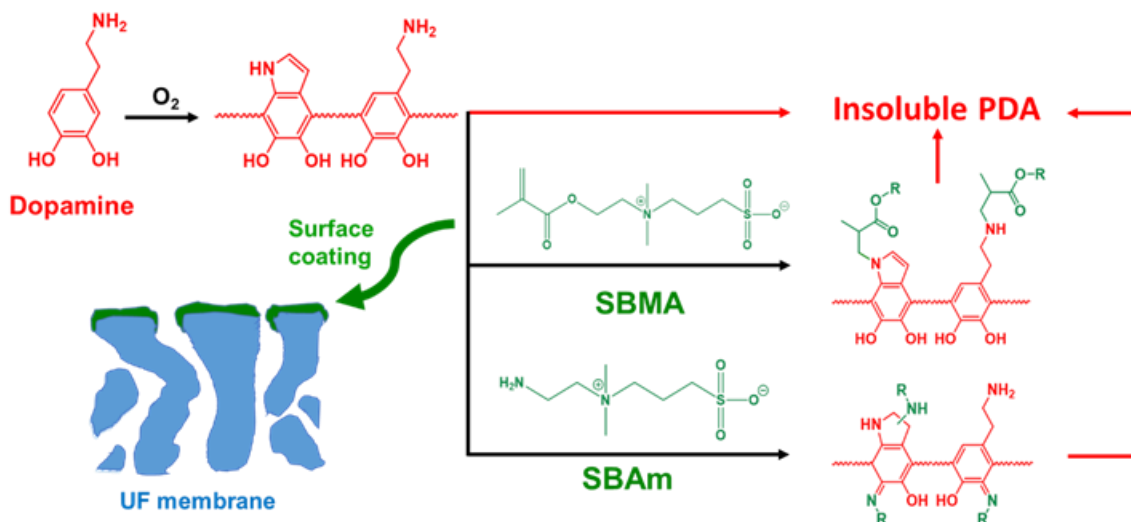


Fig. 1. Reactions between dopamine and methacrylate or amine-containing ZMs used in this study, and schematic of coating ZMs+PDA onto a UF membrane. R =  $-\text{CH}_2\text{CH}_2\text{N}^+(\text{CH}_3)_2\text{CH}_2\text{CH}_2\text{CH}_2\text{SO}_3^-$ .

content of the coating layer were determined. The optimally modified membranes with a thin layer and high SBAm content were challenged with model wastewater and compared with the pristine membranes and those modified using SBMA.

## 2. Experimental

### 2.1 Materials

Dopamine hydrochloride, Trizma base (Tris), SBMA, deuterium oxide ( $\text{D}_2\text{O}$ ), and sodium alginate (from brown algae) were purchased from Sigma-Aldrich (St. Louis, MO). SBAm and ethanol were procured from eNovation Chemicals (Green Brook, NJ) and Fisher Scientific (Waltham, MA), respectively. A polysulfone UF membrane (PSf-25) was purchased from Alfa-Laval (Warminster, PA).<sup>30</sup>

### 2.2 Surface modification

The coating conditions are denoted as  $y\text{-ZM}/x\text{-Dopa}@z\text{h}$ , where  $y$  and  $x$  represent the concentration of ZM (SBMA or SBAm) and dopamine in the coating solution (g/L), respectively, and  $z$  is the coating time (h). The desired amount of dopamine, ZM, and Tris were dissolved in Milli-Q water. The substrates to be coated (including polystyrene wells, silicon wafers, and PSf-25 membrane) were exposed to the solution for the targeted time on a rocker platform shaker (VWR International, Radnor, PA).<sup>17, 18</sup> The substrates were then rinsed with DI water before characterization.

### 2.3 Characterization of coating solutions and layers

The coating solutions were characterized using a Varian INOVA-500  $^1\text{H}$  NMR spectrometer (Varian Medical Systems, Palo Alto, CA) with  $\text{D}_2\text{O}$  as the solvent. Additionally, the solutions were drop-cast onto wafers, and the dried aggregates were examined using a focused-ion beam SEM (FIB-SEM, Auriga, ZEISS International, Germany) and attenuated total reflectance Fourier-transform infrared spectrometer (ATR-FTIR, Vertex 70, Bruker, MA).

Water contact angles were determined using a Ramé Hart goniometer (Model 190, Succasunna, NJ) and 10  $\mu\text{L}$  water

droplets. Five measurements were recorded for each sample. For the coating layers in the polystyrene wells, the thickness was determined using an F20 instrument (Filmetrics, Inc., San Diego, CA).<sup>18</sup> X-ray photoelectron spectroscopy (XPS) was used for elemental analysis of the coated wafers with a Kratos AXIS Ultra DLD Spectrometer (Kratos Analytical, Manchester, UK). The spectra were collected from spot sizes of  $300\ \mu\text{m} \times 700\ \mu\text{m}$  and analyzed using the CasaXPS software package.<sup>30</sup>

### 2.4 Membrane characterization

Pure-water permeance ( $A_w$  in  $\text{L m}^{-2}\text{h}^{-1}\text{bar}^{-1}$  or LMH/bar) of the membranes was determined using dead-end cells (Sterlitech, Kent, WA) and calculated using the following equation:

$$A_w = \frac{J_w}{\Delta p} = \frac{dV}{dt} \frac{1}{\Delta p A_m} \quad (1)$$

where  $J_w$  is the water flux (LMH),  $\Delta p$  is the trans-membrane pressure (TMP, bar),  $A_m$  is the active membrane area ( $\text{m}^2$ ), and  $dV/dt$  is the volumetric flow rate (L/h). For each membrane, the average permeance of six stamps is reported.

The molecular weight cutoffs (MWCO)<sup>31</sup> of the membranes were determined using PEG with various mass average molar masses including (1, 2, 4, 10, and 20) kDa. The MWCO is conventionally defined as the lowest molecular weight that is rejected by the membrane at a level of 90%. The rejection of the PEG ( $R$ , %) can be calculated using the following equation:

$$R = \left(1 - \frac{C_p}{C_f}\right) \times 100\% \quad (2)$$

where  $C_p$  and  $C_f$  are the PEG concentration in the permeate and feed, respectively. Both  $C_p$  and  $C_f$  were determined using a total organic carbon analyzer (Shimadzu, Japan). The membrane pore size can be estimated as the Stokes radius ( $a$ , nm) of the corresponding PEG molecule:<sup>21, 32</sup>

$$a = 16.73 \times 10^{-3} M_w^{0.557} \quad (3)$$

The antifouling properties of the UF membranes were characterized using sodium alginate as a model foulant in both

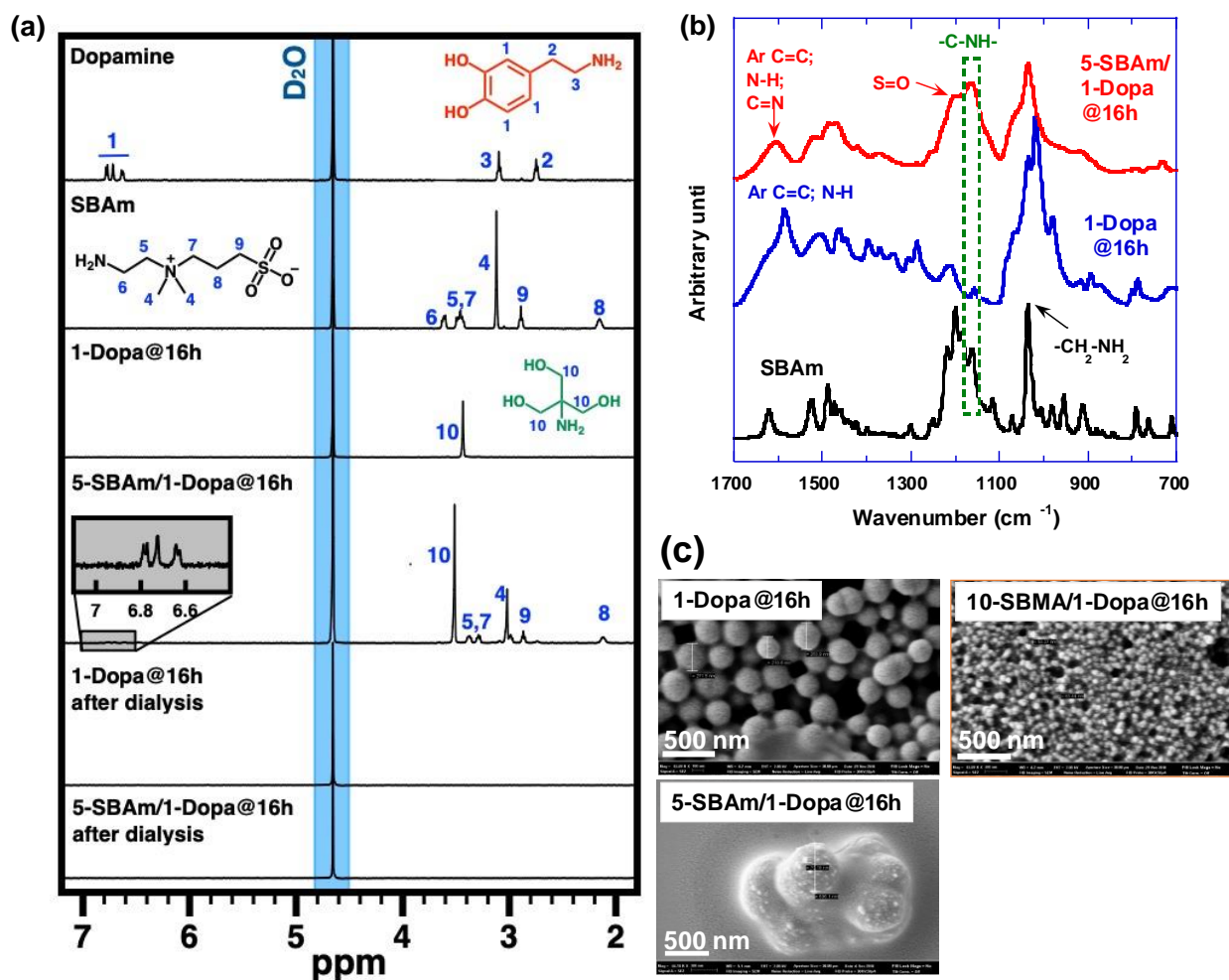


**Fig. 2** (a) <sup>1</sup>H NMR spectra of dopamine, SBAm, 1-Dopa@16h, and 5-SBAm/1-Dopa@16h in D<sub>2</sub>O. The latter two were also dialyzed using a membrane with a MWCO of 3.5 kDa. The gray inserted figure shows the aromatic protons from dopamine and soluble SBAm/PDA product. (b) FTIR spectra of SBAm and dried aggregates of 1-Dopa@16h and 5-SBAm/1-Dopa@16h. (c) SEM images of the dried PDA and ZM/PDA aggregates.

a dead-end filtration and a constant-flux crossflow geometry.<sup>33, 34</sup> For dead-end cells, a constant feed pressure was applied, and the decreased water permeance was recorded. For the constant-flux system, the feed pressure was kept constant while the permeate pressure was decreased to maintain a defined flux. The resistance to water permeation ( $R_w$ , m<sup>-1</sup>) can be calculated using eqn (4):<sup>35</sup>

$$R_w = \frac{\Delta p}{\mu_w J_w} \quad (4)$$

where  $\mu_w$  is the water viscosity. Membrane fouling is often characterized by the relative resistance defined as the ratio of the resistance at any time to the initial pure water value.

### 3. Results and discussion

#### 3.1 Reaction between the ZMs and dopamine in solutions

To elucidate the reaction of SBAm and dopamine in solutions, Fig. 2a compares <sup>1</sup>H NMR spectra of dopamine, SBAm, 1-Dopa@16h, and 5-SBAm/1-Dopa@16h in D<sub>2</sub>O. The dopamine solution was kept oxygen-free to avoid the formation of PDA, and the spectrum shows characteristic peaks at (6.6 to 6.8) ppm corresponding to the aromatic protons of dopamine, and 2.7

ppm and 3 ppm for NH<sub>2</sub>CH<sub>2</sub>CH<sub>2</sub> and NH<sub>2</sub>CH<sub>2</sub>CH<sub>2</sub>, respectively. By contrast, these peaks disappear in 1-Dopa@16h, confirming the formation of insoluble PDA in the presence of O<sub>2</sub>. The peak at ≈3.2 ppm belongs to the Tris buffer, which was used to maintain the pH of polymerization. However, 5-SBAm/1-Dopa@16h shows characteristic peaks for aromatic protons (in the gray inserted figure), suggesting the formation of soluble intermediate chemicals (cf. Fig. 1) through reaction of the amine group of SBAm with the catechol moieties of dopamine monomer/oligomer via Michael addition and with the vinyl groups of dopamine monomer/oligomer via Schiff base reaction.<sup>36</sup> The same trend is observed for 25-SBAm/1-Dopa@16h (see Fig. S1a). The 5-SBAm/1-Dopa@16h solution was dialyzed using membranes with an MWCO of 3.5 kDa for three days, and all the peaks disappear, suggesting that the soluble chemicals have molar mass less than 3.5 kDa.

Fig. 2b exhibits the FTIR spectra for SBAm and dried aggregates from the 1-Dopa@16h and 5-SBAm/1-Dopa@16h solutions. SBAm exhibits characteristic peaks of 1050 cm<sup>-1</sup> for C-N stretch corresponding to the primary amine and 1160 cm<sup>-1</sup> for S=O stretch of the sulfonate. The 1-Dopa@16h displays a peak at 1585 cm<sup>-1</sup> for aromatic C=C stretch and N-H bending,<sup>18, 22</sup> with the presence of C=N stretch as a result of Schiff base reaction,<sup>36</sup>

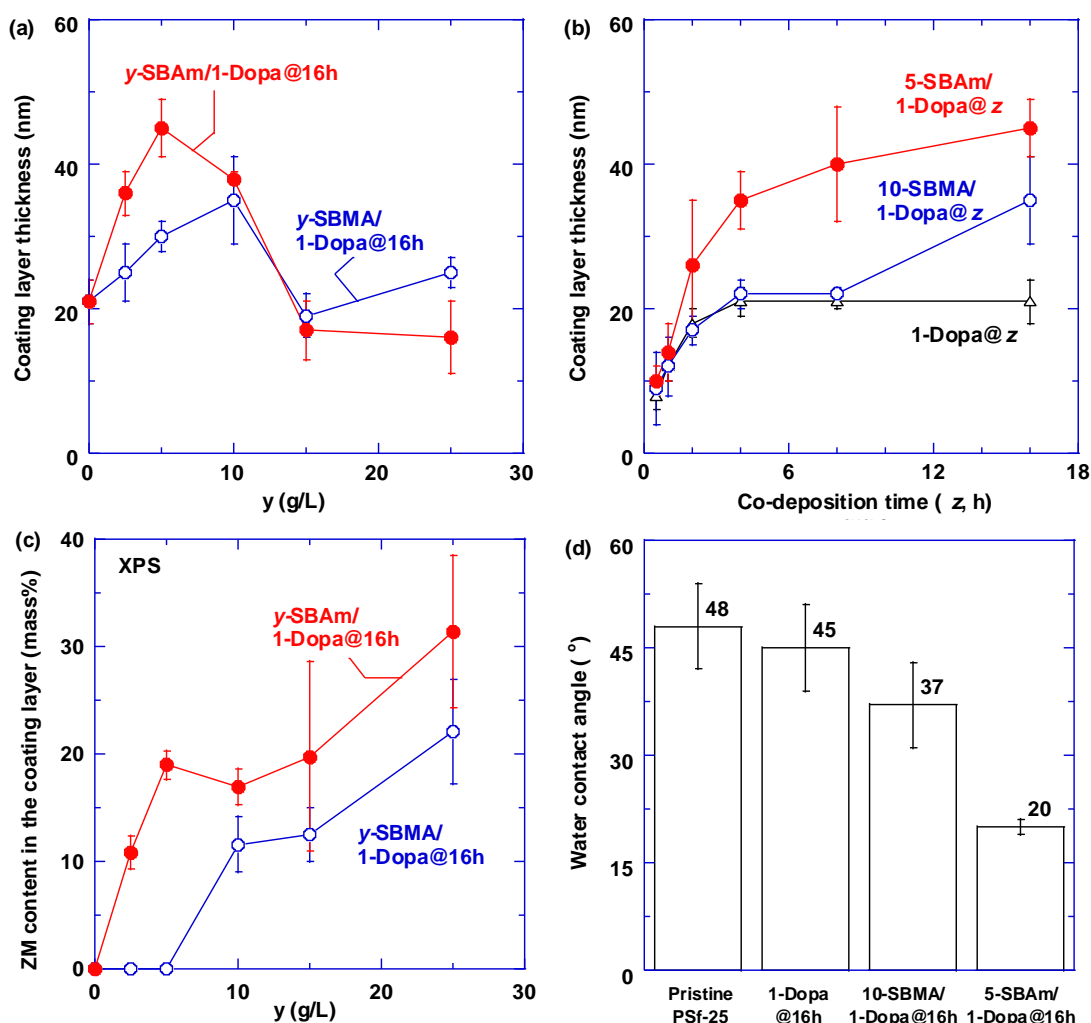


**Fig. 3** (a) Effect of the ZM content in the coating solutions ( $y$ , g/L) on the coating layer thickness when cast in polystyrene wells for  $\gamma$ -ZM/1-Dopa@16h; (b) effect of the co-deposition time ( $z$ , h) on the coating layer thickness for 1-Dopa, 10-SBMA/1-Dopa, and 5-SBAm/1-Dopa; (c) comparison of the ZM content in the coating layer on the silicon wafers for  $\gamma$ -ZM/1-Dopa@16h as a function of ZM content in the coating solutions ( $y$ , g/L); and (d) effect of representative surface modification on the water contact angle of UF membranes. The error bars represent one standard deviation of the data and are taken as the uncertainty of the measurements.

the peak shifts to  $1605\text{ cm}^{-1}$  for 5-SBAm/1-Dopa@16h. Compared with 1-Dopa@16h, 5-SBAm/1-Dopa@16h shows a strong peak at  $\approx 1150\text{ cm}^{-1}$  ascribed to  $-\text{C}-\text{NH}-$  stretch, confirming the Michael addition between SBAm and dopamine monomer/oligomer.<sup>18, 19, 26</sup>

Fig. 2c compares the SEM photos of the dried aggregates of 1-Dopa@16h, 10-SBMA/1-Dopa@16h, and 5-SBAm/1-Dopa@16h. The 1-Dopa@16h shows nanoparticle size of  $\approx 260\text{ nm}$ , while the particle size increases with the introduction of SBAm ( $\approx 650\text{ nm}$ ) and decreases with the introduction of SBMA ( $\approx 60\text{ nm}$ ), confirming the reaction between dopamine monomer/oligomer and SBAm/SBMA in the solutions. The increased particle size with adding SBAm is also confirmed by additional SEM images (cf. Fig. S1b) and dynamic light scattering (DLS) measurements (cf. Fig. S1c).

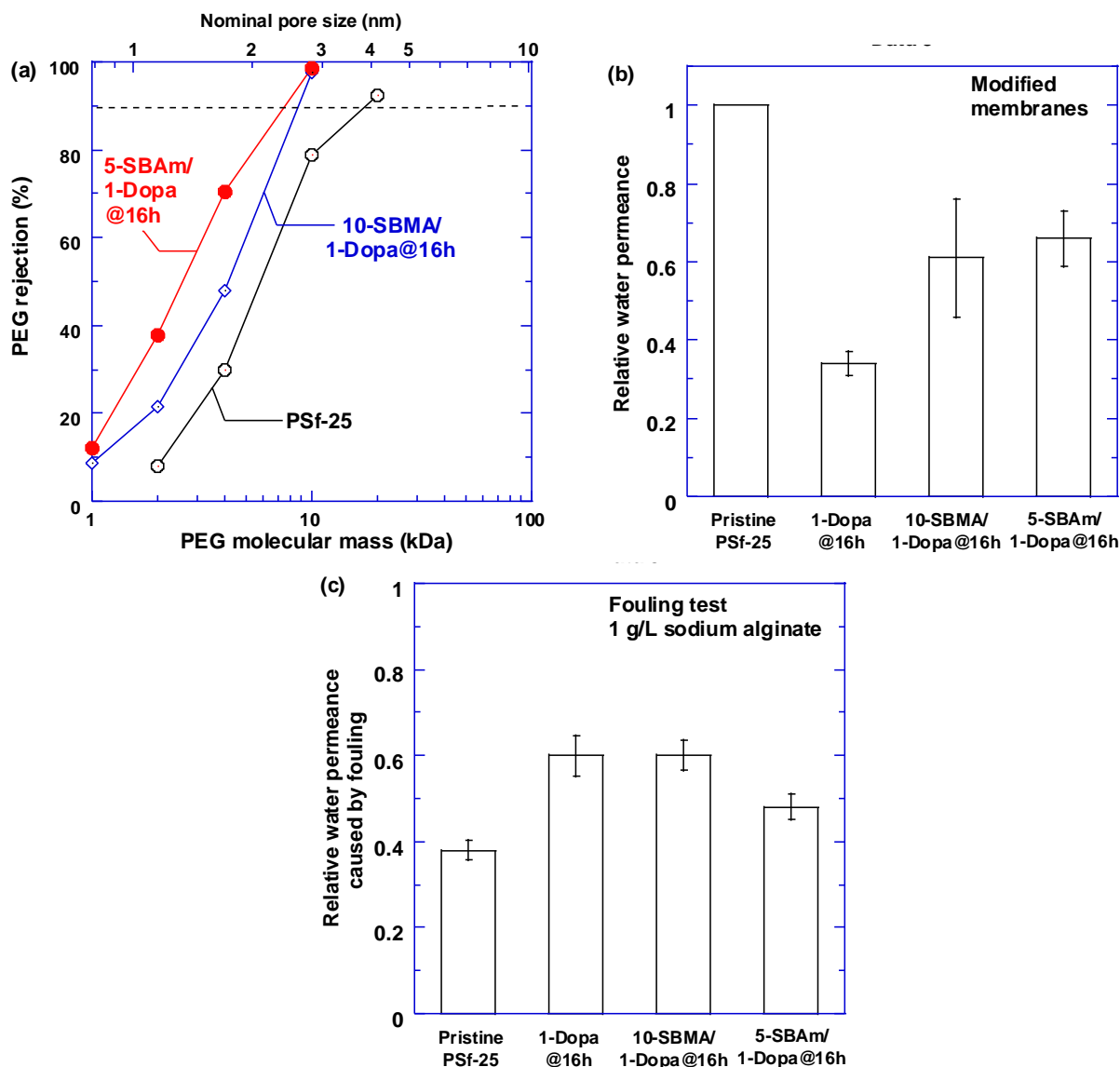
### 3.2 Characterization of coating layers

Fig. 3 displays the effect of the ZM content in the coating solution ( $y$ ) on the thickness of the coating layer ( $y$ -ZM/1-Dopa@16h) in polystyrene wells. Increasing the ZM content increases the coating layer thickness before decreasing. For

example, as the SBAm content increases from 0 to 5 g/L and 25 g/L, the thickness increases from  $21\text{ nm} \pm 3\text{ nm}$  to  $45\text{ nm} \pm 4\text{ nm}$  before decreasing to  $16\text{ nm} \pm 5\text{ nm}$ . At high ZM contents, the reaction between dopamine monomer/oligomer and ZM competes with the PDA formation, decreasing the layer thickness. Similar trends have been reported for SBMA.<sup>19</sup> The layer thickness reaches a maximum at  $y$  values of 10 g/L for SBMA and 5 g/L for SBAm, and these conditions were chosen for further studies.

Increasing the co-deposition time ( $z$ ) increases the coating layer thickness before leveling off for 10-SBMA/1-Dopa and 5-SBAm/1-Dopa, as shown in Fig. 3b. SBAm leads to thicker coating layers than SBMA, indicating that amine groups are more effective than methacrylate groups in grafting the zwitterion to the dopamine.

Fig. 3c shows the ZM content in the coating layer on the wafers determined using XPS, and the atomic compositions are recorded in Table S1. Increasing the  $y$  value continuously increases the ZM content, in contrast to the trend of the coating layer thickness (which peaks at certain  $y$  values). On the other hand, both effects are desirable for membrane surface



**Fig. 4** Effect of surface modification on (a) PEG rejection curves as a function of the PEG  $M_w$  and (b) the relative water permeance (defined as the pure water permeance ratio of the modified membrane to the pristine one), and (c) the water permeance reduction percentage when challenged with a 1 g/L sodium alginate solution. For Fig. 4b, the error bars represent one standard deviation of the data and are taken as the uncertainty of the measurements. For Fig. 4c, the uncertainty for each sample is calculated using an error propagation analysis.<sup>37</sup>

modification, i.e. thinner and more hydrophilic coating to achieve antifouling properties without dramatically increasing transport resistance. SBAm deposits more readily than SBMA in the coating layer. For example, at  $\gamma = 25$  g/L, the coating layer has 31 mass% SBAm and only 22 mass% SBMA, corresponding to 25 mass% and 13 mass% zwitterionic groups (i.e.  $-N^+(\text{CH}_3)_2\text{CH}_2\text{CH}_2\text{CH}_2\text{SO}_3^-$ ), respectively.

The ZM grafting on the membranes decreases the water contact angle (cf. Fig. 3d), indicating improved hydrophilicity, which is consistent with the thicker layer and higher ZM content for the SBAm grafting.

### 3.3 Effect of surface modification on membrane performance

Fig. 4a illustrates the rejection curves as a function of PEG molar mass for the pristine and modified PSf-25 UF membranes. The pristine PSf-25 membrane shows a MWCO of 17.5 kDa, which is comparable with that (25 kDa) given by the manufacturer, while

the MWCO decreases to 8.7 kDa for 10-SBMA/1-Dopa@16h and 7.5 kDa for 5-SBAm/1-Dopa@16h. Accordingly, the nominal pore size decreases from 3.9 nm to 2.6 nm for 10-SBMA/1-Dopa@16h and 2.4 nm for 5-SBAm/1-Dopa@16h. The decreasing order of the pore size is consistent with the thickness increase of the coating layer.

Surface modification generally decreases water permeance because of the increased resistance. Fig. 4b shows that the relative water permeance (defined as the permeance ratio of the modified membrane to the pristine one) is below 1, indicating increased resistance to water permeation. Interestingly, compared with the 1-Dopa@16h, adding ZMs increases the water permeance because of the improved hydrophilicity. Fig. 4c illustrates the effect of surface modification on the antifouling properties when challenged by 1 g/L sodium alginate solution.

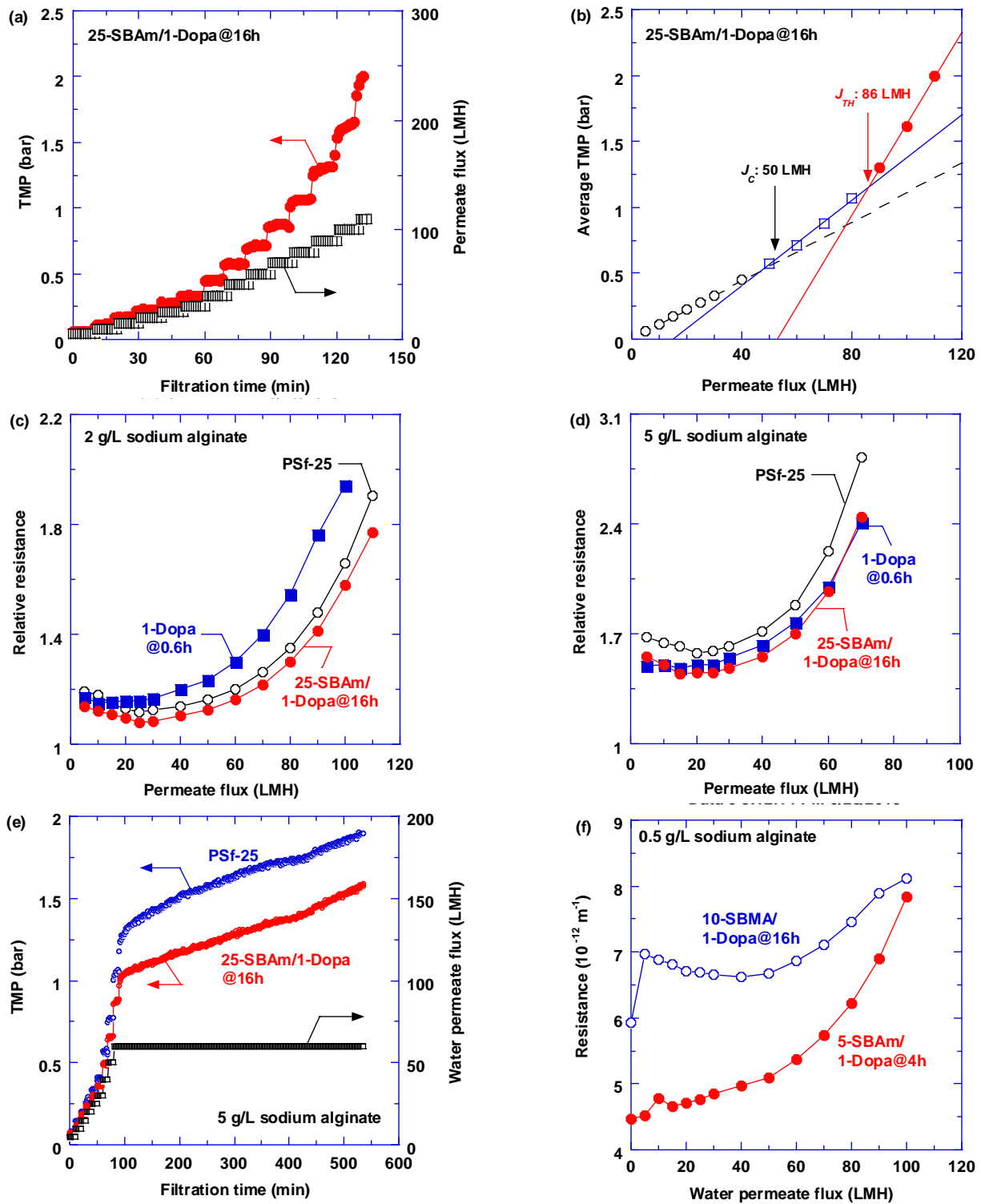


**Fig. 5** (a) Flux-stepping experiment and (b) determination of the critical and threshold flux for 25-SBAm/1-Dopa@16h examined with 2 g/L sodium alginate. Effect of the permeate flux on the relative resistance with (c) 2 g/L and (d) 5 g/L sodium alginate for three membranes, PSf-25, 1-Dopa@zh, and 25-SBAm/1-Dopa@16h. (e) Flux stepping and long-term fouling experiments for PSf-25 and 25-SBAm/1-Dopa@16h using a 5 g/L sodium alginate. (f) Effect of the permeate flux on the resistance with 0.5 g/L sodium alginate in two membranes, 5-SBAm/1-Dopa@4h, and 10-SBMA/1-Dopa@16h. The feed pressure was 2.4 barg (0.24 MPa), and the Reynolds number was  $\approx 1600$ .

The modified membranes exhibit a relative water (defined as the ratio of permeance during the fouling test to that with pure water) of 0.48 to 0.60, greater than the pristine one (0.38), confirming the improved antifouling properties by PDA and ZM coating.

Industrial membranes are often operated at constant flux (for stable productivity) at or slightly below the threshold flux ( $J_{TH}$ , defined as the flux above which significant fouling occurs).<sup>35, 38</sup> Fig. 5a illustrates the flux stepping method to obtain  $J_{TH}$  for 25-SBAm/1-Dopa@16h with 2 g/L sodium alginate solution. During the test, each flux was held for 10 min while

continuously recording the TMP. Fig. 5b shows the average TMP as a function of the water flux. Three linear regions are considered with an  $R^2 > 0.99$ . The intersection between the second and third region is defined as the  $J_{TH}$ , while the intersection between the first and second region is the critical flux ( $J_C$ , the flux below which the fouling rate is negligible).<sup>21, 39</sup>

Fig. 5c compares the fouling behavior of three membranes, PSf-25, 1-Dopa@0.3h, and 25-SBAm/1-Dopa@16h, which show comparable pure-water permeance of (106, 97, and 99) LMH/bar, respectively, and comparable  $J_{TH}$  values of (86, 68, and 86) LMH/bar (cf. Fig. S2), respectively. Therefore, a comparison of these membranes can provide useful information regarding the impact of surface modification on the antifouling properties. At fluxes below  $J_C$ , the relative resistance does not change for all three membranes (cf. Fig. 5c) because of negligible fouling. At higher fluxes, the relative resistance increases with increasing water flux, and the increasing rate of resistance becomes more rapid due to the increasingly severe fouling. The membrane modified by SBAm shows the lowest relative resistance, confirming the benefit of the SBAm in improving the antifouling properties. Fig. 5d compares the relative resistance at 5 g/L sodium alginate in the pristine PSf-25 and membranes modified by 1-Dopa@0.6h and 25-SBAm/1-Dopa@16h. Both modified membranes show significantly lower relative resistance than the PSf-25, further validating the benefits of the zwitterion grafting.

The long-term performance of the membranes when challenged with 5 g/L sodium alginate solution is illustrated in Fig. 5e. The PSf-25 and 25-SBAm/1-Dopa@16h exhibit pure-water permeance of 146 LMH/bar and 138 LMH/bar, respectively, making them ideal for comparison. At the initial flux-stepping stage, the SBAm-modified membrane exhibits 15 % to 25 % lower resistance than the pristine one. During the continuing test of  $\approx 8$  h at 60 LMH, the SBAm-modified membrane again shows lower resistance, confirming the stability and improved antifouling properties of the surface modification. The superior antifouling behavior of the SBAm-modified membrane over the PDA-modified one is also demonstrated in Fig. S2d.

Fig. 5f compares the antifouling properties of 10-SBMA/1-Dopa@16h and 5-SBAm/1-Dopa@4h with 0.5 g/L sodium alginate solution. Despite the same coating layer thickness of both coatings (i.e. 35 nm, as shown in Fig. 3b), the SBAm-modified membrane exhibits lower resistance than the SBMA-modified one, though the difference diminishes as the flux increases above  $J_{TH}$ . Such a result demonstrates that SBAm is more effective than SBMA for surface-grafting to enhance antifouling properties.

## Conclusions

We demonstrate a facile approach to graft zwitterions (up to 31 mass% in thin layers of  $< 20$  nm) on the membrane surface to improve antifouling properties. The amine-functionalized ZMs (i.e. SBAm) can be co-deposited with dopamine on a variety of surfaces in aqueous solution at  $\approx 22$  °C. The reaction between SBAm and dopamine monomer/oligomer is confirmed by <sup>1</sup>H NMR spectroscopy, SEM, and FTIR. The grafting of the

zwitterions in the coating layers is also confirmed by XPS. SBAm leads to a thicker coating layer and higher zwitterion content than SBMA, suggesting that amine groups are more effective than methacrylate counterparts to graft zwitterions. In a constant-flux system, SBAm-modified membranes show 15 % to 25 % lower resistance to water permeation than the SBMA-modified analog and pristine one, confirming the effectiveness of the grafting of amine-functionalized zwitterions to enhance membrane antifouling properties.

## Conflicts of interest

The authors declare no conflicts of interest.

## Acknowledgments

We acknowledge the financial support from the U.S. National Science Foundation (NSF Award No. 1635026) and Department of Energy Small Business Innovation Research program (Award No. DE-SC-0017077). This work is an official contribution of the National Institute of Standards and Technology and not subject to copyright in the United States.

## References

1. D. Miller, D. Dreyer, C. Bielawski, D. Paul and B. Freeman, *Angew. Chem. Int. Ed.*, 2017, **56**, 4662-4711.
2. N. Shahkaramipour, T. Tran, S. Ramanan and H. Lin, *Membranes*, 2017, **7**, 13.
3. R. Zhang, Y. Liu, M. He, Y. Su, X. Zhao, M. Elimelech and Z. Jiang, *Chem. Soc. Rev.*, 2016, **45**, 5888-5924.
4. P. Kaner, A. V. Dudchenko, M. S. Mauter and A. Asatekin, *J. Mater. Chem. A*, 2019, **7**, 4829-4846.
5. R. Yang, P. Moni and K. K. Gleason, *Adv. Mater. Interfaces*, 2015, **2**, 1400489.
6. D. Hong, H.-C. Hung, K. Wu, X. Lin, F. Sun, P. Zhang, S. Liu, K. E. Cook and S. Jiang, *ACS Appl. Mater. Interf.*, 2017, **9**, 9255-9259.
7. Z. Liu, Q. Jiang, Z. Jin, Z. Sun, W. Ma and Y. Wang, *ACS Appl. Mater. Interf.*, 2019, **11**, 14408-14417.
8. D. M. Davenport, J. Lee and M. Elimelech, *Sep. Purif. Technol.*, 2017, **189**, 389-398.
9. Q. Li, J. Imbrogno, G. Belfort and X. L. Wang, *J. Appl. Polym. Sci.*, 2015, **132**, 41781.
10. Y.-H. Chiao, A. Sengupta, S.-T. Chen, S.-H. Huang, C.-C. Hu, W.-S. Hung, Y. Chang, X. Qian, S. R. Wickramasinghe and K.-R. Lee, *Sep. Purif. Technol.*, 2019, **212**, 316-325.
11. M. Yi, C. H. Lau, S. Xiong, W.-J. Wei, R.-Z. Liao, L. Shen, A. Lu and Y. Wang, *ACS Appl. Mater. Interf.*, 2019, **11**, 15698-15708.
12. H. Sun, Y. Zhang, H. Sadam, J. Ma, Y. Bai, X. Shen, J.-K. Kim and L. Shao, *J. Membr. Sci.*, 2019, **582**, 1-8.
13. N. Ma, J. Cao, H. Li, Y. Zhang, H. Wang and J. Meng, *Polymer*, 2019, **167**, 1-12.
14. H. Lee, S. M. Dellatore, W. M. Miller and P. B. Messersmith, *Science*, 2007, **318**, 426-430.
15. D. R. Dreyer, D. J. Miller, B. D. Freeman, D. R. Paul and C. W. Bielawski, *Chem. Sci.*, 2013, **4**, 3796-3802.
16. W. Qiu, H. Yang and Z. Xu, *Adv. Colloid Interface Sci.*, 2018, **256**, 111-125.

17. N. Shahkaramipour, C. K. Lai, S. R. Venna, H. Sun, C. Cheng and H. Lin, *Ind. Eng. Chem. Res.*, 2018, **57**, 2336-2345.
18. N. Shahkaramipour, S. N. Ramanan, D. R. Fister, E. Park, S. R. Venna, H. Sun, C. Cheng and H. Lin, *Ind. Eng. Chem. Res.*, 2017, **56**, 9202-9212.
19. C. Zhang, M. Ma, T. Chen, H. Zhang, D. Hu, B. Wu, J. Ji and Z. Xu, *ACS Appl. Mater. Interf.*, 2017, **9**, 34356-34366.
20. C. Chang, K. W. Kolewe, Y. Li, K. I., B. D. Freeman, K. R. Carter, J. D. Schiffman and T. Emrick, *Adv. Mater. Interfaces*, 2016, **3**, 1500521.
21. A. Kirschner, C. Chang, S. Kasemset, T. Emrick and B. D. Freeman, *J. Membr. Sci.*, 2017, **541**, 300-311.
22. R. Zhou, P. Ren, H. Yang and Z. Xu, *J. Membr. Sci.*, 2014, **466**, 18-25.
23. C.-Y. Liu and C.-J. Huang, *Langmuir*, 2016, **32**, 5019-5028.
24. W. Qiu, G. Wu and Z. Xu, *ACS Appl. Mater. Interf.*, 2018, **10**, 5902-5908.
25. W. Qiu, H. Yang, L. Wan and Z. Xu, *J. Mater. Chem. A*, 2015, **3**, 14438-14444.
26. H. Yang, K. Liao, H. Huang, Q. Wu, L. Wan and Z. Xu, *J. Mater. Chem. A*, 2014, **2**, 10225-10230.
27. B. D. McCloskey, H. B. Park, H. Ju, B. W. Rowe, D. J. Miller, B. J. Chun, K. Kin and B. D. Freeman, *Polymer*, 2010, **51**, 3472-3485.
28. S. N. Ramanan, N. Shahkaramipour, T. Tran, L. Zhu, S. R. Venna, C.-K. Lim, A. Singh, P. N. Prasad and H. Lin, *J. Membr. Sci.*, 2018, **554**, 164-174.
29. Y. Du, W. Z. Qiu, Y. Lv, J. Wu and Z. K. Xu, *ACS Appl. Mater. Interf.*, 2016, **8**, 29696-29704.
30. *Equipment and instruments or materials are identified herein to adequately specify the experimental details.*
31. *Such identification does not imply recommendation by the National Institute of Standards and Technology, nor does it imply the materials are necessarily the best available for the purpose.*
32. *The appropriate SI unit is molecular mass cutoff. However, the conventional notation, molecular weight cutoff or MWCO, has been employed for this publication as it is the accepted terminology in the field.*
33. S. Kasemset, L. Wang, Z. He, D. J. Miller, A. Kirschner, B. D. Freeman and M. M. Sharma, *J. Membr. Sci.*, 2017, **522**, 100-115.
34. T. Tran, Y. Tu, S. Hall-Laureano, C. Lin, M. Kawy and H. Lin, *Submitted*, 2019.
35. D. J. Miller, D. R. Paul and B. D. Freeman, *Rev. Sci. Instrum.*, 2013, **84**, 035003.
36. D. J. Miller, S. Kasemset, L. Wang, D. R. Paul and B. D. Freeman, *J. Membr. Sci.*, 2014, **452**, 171-183.
37. J. H. Ryu, P. B. Messersmith and H. Lee, *ACS Appl. Mater. Interf.*, 2018, **10**, 7523-7540.
38. P. R. Bevington and D. K. Robinson, *Data Reduction and Error Analysis for the Physical Sciences*, McGraw-Hill, Inc., New York, second edn., 1992.
39. A. Y. Kirschner, Y.-H. Cheng, D. R. Paul, R. W. Field and B. D. Freeman, *J. Membr. Sci.*, 2019, **574**, 65-75.
40. D. J. Miller, S. Kasemset, D. R. Paul and B. D. Freeman, *J. Membr. Sci.*, 2014, **454**, 505-515.



## Supplemental Information

### **Maximizing the grafting of zwitterions onto the surface of ultrafiltration membranes to improve antifouling properties**

Nima Shahkaramipour<sup>1</sup>, Amin Jafari<sup>1</sup>, Thien Tran<sup>1</sup>, Christopher M. Stafford<sup>2</sup>, Chong Cheng<sup>1</sup>, and Haiqing Lin<sup>1,\*</sup>

<sup>1</sup>Department of Chemical and Biological Engineering, University at Buffalo,  
The State University of New York, Buffalo, NY 14260, USA

<sup>2</sup>Materials Science & Engineering Division, National Institute of Standards and Technology (NIST), 100  
Bureau Drive, Gaithersburg, MD 20899, USA

## Reaction between the ZMs and dopamine in solutions

Fig. S1a shows the  $^1\text{H}$  NMR spectrum of the 25-SBAm/1-Dopa@16h in  $\text{D}_2\text{O}$ . The peaks in the grey area confirm the reaction between SBAm and dopamine as they are absent in the 1-Dopa@16h spectrum (see Fig. 2a in the manuscript).

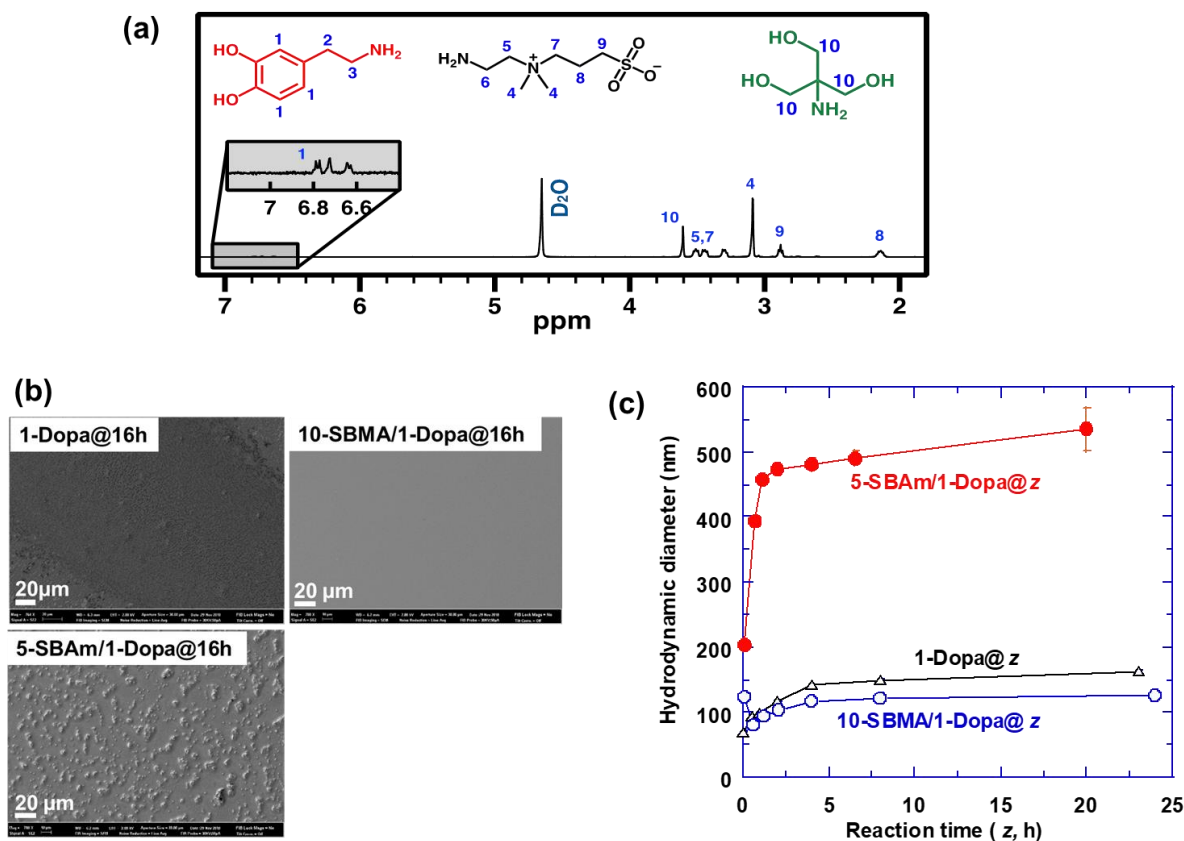


**Fig. S1** (a)  $^1\text{H}$  NMR spectrum of 25-SBAm/1-Dopa@16h in  $\text{D}_2\text{O}$ . (b) SEM images of the dried PDA and ZM/PDA aggregates. (c) The hydrodynamic diameter of the aggregates from the solutions prepared with PDA and ZM/PDA, as assessed by dynamic light scattering (DLS).

Fig. S1b exhibits the dried aggregates from the solution using a low SEM magnification. 5-SBAm/1-Dopa@16h forms larger aggregates than 1-Dopa@16h and 10-SBMA/1-Dopa@16h. For the last two conditions, the aggregates can be barely seen under such low magnification.

Fig. S1c shows the effect of the reaction time on the hydrodynamic diameter of the aggregates in the solutions of PDA and ZM/PDA, which were determined using DLS with a Zetasizer Nano ZS90 (Malvern Panalytical, Westborough, MA). For all solutions, the aggregate size increases with time before leveling off. Consistent with the SEM results, the 5-SBAm/1-Dopa@16h forms larger aggregates than 1-Dopa@16h and 10-SBMA/1-Dopa@16h.

## Characterization of coating layers

Table S1 summarizes the atomic composition and *S/C* ratio of the coating layers on Si wafers determined using XPS. The wafers were used due to the simplicity in the coating and XPS measurement with an assumption that the layer compositions are independent of the substrate. However, the coating layer is thinner on the wafers than on the polystyrene wells. For example, the coating layer of 15-SBAm/1-Dopa@16h and 25-SBAm/1-Dopa@16h has a thickness of  $5\pm 3$  nm and  $8\pm 1$  nm thickness, respectively, which are thinner than those ( $\approx 20$  nm) on the polystyrene wells. Consequently, the coating layers derived from ZM contents of 15 g/L and 25 g/L show high Si content from the wafers.

Table S1 demonstrates that introducing SBAm or SBMA in the coating solutions enhances the *S/C* ratio, indicating the increase in the zwitterion content in the coating layers. 15-SBAm/1-Dopa@16h and 25-SBAm/1-Dopa@16h show high uncertainty of *S/C* ratio because of the use of less sensitive S 2s peak, instead of the primary S 2p peak as was used for the other measurements. The S 2p overlaps with the Si 2s signal.

**Table S1.** Elemental composition (atomic%) of the coating layers on the Si wafers determined using XPS.

Samples	C 1s	O 1s	N 1s	S 2p	Si 2s	<i>S/C</i>
Bare Si wafer	7.87	31.76	---	---	60.37	0
1-Dopa@16h	71.12	20.90	7.72	---	0.25	0
2.5-SBMA/1-Dopa@16h	71.21	20.20	7.59	---	1.00	0
5-SBMA/1-Dopa@16h	70.18	20.67	7.51	---	1.63	0
10-SBMA/1-Dopa@16h	67.32	23.72	6.47	0.55	1.94	0.008 $\pm$ 0.002
15-SBMA/1-Dopa@16h	57.09	23.03	5.69	0.50	13.68	0.009 $\pm$ 0.002
25-SBMA/1-Dopa@16h	41.62	25.85	3.81	0.67	28.06	0.016 $\pm$ 0.004
2.5-SBAm/1-Dopa@16h	70.32	20.50	8.46	0.72	---	0.010 $\pm$ 0.002
5-SBAm/1-Dopa@16h	68.34	22.17	8.23	1.27	---	0.019 $\pm$ 0.001
10-SBAm/1-Dopa@16h	67.82	23.31	7.76	1.12	---	0.016 $\pm$ 0.002
15-SBAm/1-Dopa@16h	55.06	25.43	6.21	1.08*	12.22	0.020 $\pm$ 0.009
25-SBAm/1-Dopa@16h	39.40	27.32	4.94	1.27*	27.07	0.032 $\pm$ 0.008

\*S 2s peak was used for the measurement, instead of S 2p peak.

## Characterization of membrane performance

Fig. S2a shows the flux stepping results for the pristine PSf-25 and the one modified with 1-Dopa@0.3h when challenged with a 2 g/L sodium alginate solution in a constant-flux crossflow system. The determination of the critical and threshold flux is shown in Figs. S2b and S2c, respectively. The PDA modification decreases the critical and threshold flux because of the decreased water permeance and pore size.

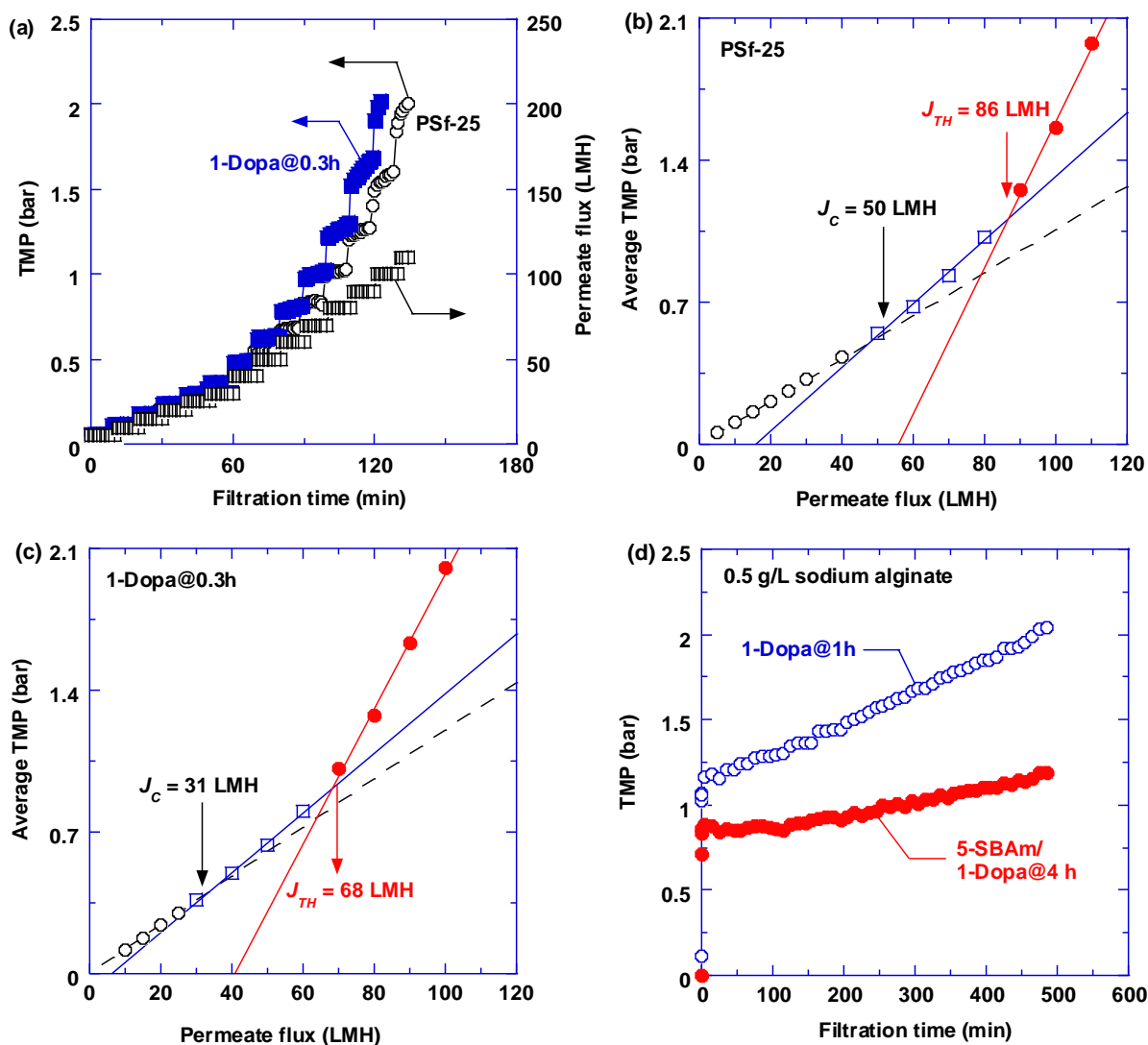


**Fig. S2.** (a) Flux stepping experiment for PSf-25 and 1-Dopa@0.3h. Determination of the critical and threshold flux for (b) PSf-25 and (c) 1-Dopa@0.3h. (d) Comparison of long-term fouling experiment at 73 LMH for 1-Dopa@1h and 5-SBAm/1-Dopa@4h. In these measurements, the feed pressure was 2.4 barg (0.24 MPa), and the Reynolds number was  $\approx 1600$ .

Fig. S2d compares the long-term fouling test for 1-Dopa@1h and 5-SBAm/1-Dopa@4h using 0.5 g/L sodium alginate. Although both membranes show very similar pure-water permeance ( $\approx 90$  LMH), the SBAm modified one exhibits higher critical and threshold flux (i.e. 40 LMH and 76 LMH, respectively) than the PDA modified one (i.e. 23 LMH and 56 LMH, respectively). When operated at 73 LMH, 5-SBAm/1-Dopa@4h shows less increase in TMP (i.e.  $\approx 36\%$ ) than 1-Dopa@1h (i.e.  $\approx 71\%$ ). After the fouling test, the crossflow system was rinsed with DI water, and the SBAm modified membrane recovers 80% of its initial pure-water permeance, much higher than that for the PDA modified one (i.e. 56%).